ELSEVIER

Cement & Concrete Composites 23 (2001) 133–151

Cement & Concrete Composites

www.elsevier.com/locate/cemconcomp

Image analysis and mathematical morphology for civil engineering materials

Michel Coster, Jean-Louis Chermant *

LERMAT, URA CNRS 1317, ISMRA, 6 Boulevard Maréchal-Juin, 14050 Caen Cedex, France

Abstract

The scope of this paper is to present the main tools of image analysis to investigate materials and, specially, civil engineering ones. First the acquisition methods are described. The different operators for filtering, segmentation and binary image processing are presented and illustrated on different images. The influence of the observation field on these operators and the bias correction is also introduced. Then the problem of the parametrical characterization is presented: stereological parameters and functions related to size distributions, dispersion and anisotropy. Finally, the model methods based on image analysis are recalled. Some annexes illustrate this paper to precise main basic notions to understand the morphological tools. © 2001 Elsevier Science Ltd. All rights reserved.

Keywords: Automatic image analysis; Image processing; Mathematical morphology; Acquisition; Anisotropy; Dispersion; Extraction; Filtering; Granulometry; Measurements; Modelling; Morphological parameters; Segmentation

1. Introduction

Image processing and analysis are very powerful tools when morphological information is required to understand the behaviour of a material, or to help a physician in its diagnosis, or to sort out objects, etc. Civil engineering materials are also concerned with this type of characterization. In this paper, we shall briefly present the main principles of image processing and analysis applied to (civil engineering) materials, their constraints, their procedures, and the main tools to be used. This must help in the understanding of the various papers of this special issue on image analysis applied to civil engineering materials.

2. Main principles

Image analysis applied to materials, and more specially civil engineering ones, can be divided into three main steps:

- image acquisition,
- extraction of the pertinent characteristics and image segmentation,
- extension of this information via parameters or functions, and/or modelling.

During such analysis, problems of statistical and stereological nature have to be solved.

Statistical problems are related to the size of the images compared to the structure [1], their position and number. Due to the observation scale used, the morphology of a material presents generally a random character, and can only be analysed in a frame of measurements of reduced size. This frame has to be large enough to observe the largest features and the size of the pixel small enough to detect the smallest details. A correct magnification will be the result of a compromise. Thereafter the minimum number of frames of measurements to be analysed must be determined and a sampling plan chosen. For this purpose geostatistic methods can be used [2].

Stereological problems are also to be solved as in situ analysis (3D). Generally, this is not possible on such materials as one mainly works on a plane section (2D). So stereological parameters and relationships can be used to access 3D characteristics from 2D analysis [3–5].

3. Sampling preparation and choice of the image source

The sampling preparation and the choice of the image source will depend on the nature of the material: either bulk or particulate material.

* Corresponding author. Tel.: +33-231-452-664; fax: +33-231-452-660.

PII: S0958-9465(00)00058-5

3.1. Bulk materials

Regarding the probe for bulk materials, one must know if the material is opaque or transparent to the photons (visible light or X-rays) or electrons (scanning, transmission electron microscopies). Civil engineering materials are relatively opaque to photons of the visible wavelength, but X-rays can penetrate a certain thickness. Using an optical microscope one can use either a thin slice as in petrography, or work by reflection on a polished section. Then an image of a 2D section is obtained from a 3D structure. A 3D reconstruction from X-rays observation can be performed using tomography equipments as for biology, but the X-ray penetration remains low and this type of investigation is rarely used [6–9].

Of course, the two main modes of acquisition are scanning electron microscopy (SEM) and optical systems using visible light. For this last mode, many types of equipments exist and their choice will depend on the magnification required. For higher magnification, a black and white or colour camera connected to a microscope will be utilized.

Macrographic bench or a flat scanner are used for the macroscopic scale. The progress in multimedia systems leads to the development of high performance scanners with more than 4000 pixels per inch: they compete with the optical microscopes in the field of low magnification with a size of image much larger. In both cases colour or grey tone images can be used.

Regarding the SEM, several types of signals can be used: secondary, back scattered electrons, X-ray images, etc. Using a numerical SEM, several images of the same area are obtained, corresponding to multimodal images. This can enable to select, for example, specific phases and to perform a threshold without difficulties [10].

3.2. Particulate materials

If the analysis is performed on a particulate material, the morphological investigation will mainly concern the outline of the particles, as they have to be set on an adequate support. However the lack of depth of focus of the optical microscopes (confocal microscopy is little used in material science) is to be taken into account. With optical microscopy, one only accesses reflected or transmitted images to analyse the 2D silhouette of particles. The observation by SEM is only by reflection. Due to its depth of focus, more morphological information can be attained than by optical microscopy. Nevertheless, it is a pseudo-relief which is analysed, which limits this type of characterization.

To investigate the internal structure of a particulate material, it must be embedded in a resin to obtain a polished section.

4. Acquisition and nature of images

The acquisition of an image corresponds to a transformation of a real image in number: so, a numerical image is obtained the nature of which will closely depend on its source. Practically two types of images must be distinguished: grey tone images and colour images classically defined from three channels. SEM multimodal images are closed to colour images, as several functions can be associated to each pixel. Nevertheless, the comparison cannot go any further as the colour image is in fact defined in a vectorial space (see Appendix A): that will possibly be taken into account in the image processing.

5. Extraction of features and image segmentation

The aim of this step is to improve the quality of images or to evidence some specific characteristics. That includes the parameter extraction and the restoration of images, which are noisy, or with defects.

So a filtering process must be used to improve the quality of such images.

The segmentation consists of constructing a symbolic representation of the images, i.e., to define a cartography of the image to describe the homogeneous areas according to one or some attributes (features) chosen a priori.

5.1. Filtering

Whatever is the acquisition mode, image processing must be used on the one hand to eliminate the noise related to the acquisition system, and on the other hand to increase the difference in the contrast between the phases or the object classes which are to be extracted. Generally, noise appears for a frequency much larger than that of the pertinent information. So low-pass filter will eliminate that noise.

Sometimes it is more interesting to extract the contour (outline) of objects than the objects themselves. Then it will be necessary to enhance these outlines which are generally recognizable by their large variation in the colour or the grey tone levels. They are high-pass filters. Outside their role in the elimination of noise or enhancement of outlines, filters can be classified as a function of their mathematical properties. One mainly distinguishes:

- linear filters,
- rank filters,
- morphological filters.

5.1.1. Linear filters

Linear filters possess a characteristic of additivity (hence their names), specific to their mathematical structure. Convolution products and filtering by Fourier transform (FT) belong to this class [11].

The convolution product is defined by:

$$g(i) = f(i) * v(i) = \frac{\sum_{j=0}^{n} f(i-j)v(j)}{\sum_{j=0}^{n} v(j)} \quad \text{for } \sum_{j=0}^{n} v(j) \neq 0, \tag{1}$$

$$g(i) = f(i) * v(i) = \sum_{j=0}^{n} f(i-j)v(j) \quad \text{for } \sum_{j=0}^{n} v(j) = 0. \tag{2}$$

In these relationships, $f(i)$ is the value of the pixel i of the image source, and $g(i)$ that corresponding to the filtered image. j is a classification index of the coefficient $v(j)$ of the neigbourhood function. When the sum of these coefficients is nul, high-pass (gradient or Laplacian) filters are defined. Generally, the neighbourhood function corresponds to 3×3 or 5×5 matrix. Fig. 1(a) presents a composite structure and Fig. 1(b) the effect of a simple mean filter of 5×5 size on image 1a.

5.1.2. Rank filters

With rank filters, values of pixels $(i-j)$ close to common pixel i of image f are classified. Thus a distribution is defined and a characteristic position distribution is attributed to the pixel i of image g. Generally the median value is taken (filtering by the median), i.e., that which corresponds to the grey tone level such as the number of darkest and brightest pixels in the investigated neighbourhood will be the same. These filters do not possess particular properties, but

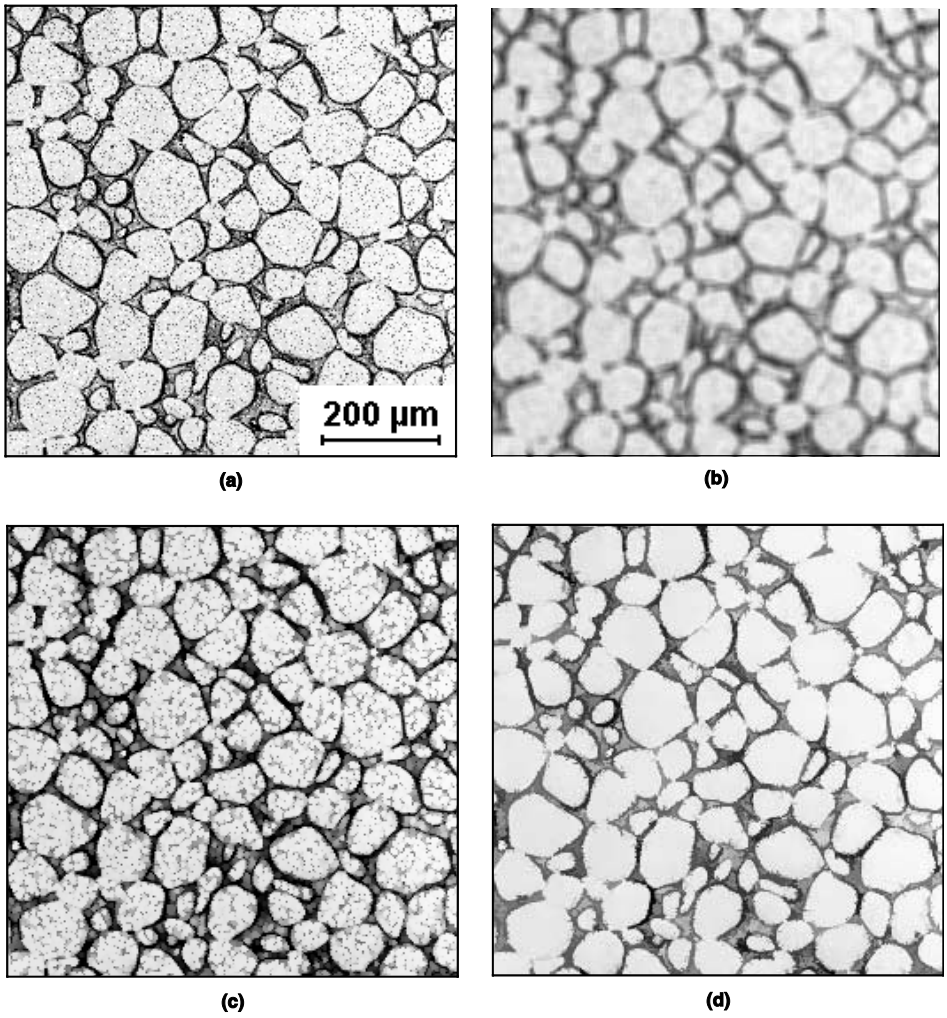

Fig. 1. (a) Metallographic surface of a composite. (b) Effect of a 5×5 mean filter on image 1a. (c) Effect of an opening filter on image 1a. (d) Filtering by reconstruction of the opened image by the closed one of size 1 on image 1a.

they are relatively efficacious. When the maximum or the minimum value of the distribution is chosen, rank filters are equivalent to dilations or erosions. Fig. 2(a) shows the effect of a median filter on image 1a.

5.1.3. Morphological filters

The methods of morphological filtering using operators of mathematical morphology [12,13] are divided in two classes: morphological filters [14] and filters based on morphological residues [15]. The standards of morphological filters are the morphological opening and closing. These operators are themselves constructed from the two main basic operators of mathematical morphology: erosion and dilation [5,12], (see Appendix B). The morphological opening is the erosion of the function f by a structuring element B of size λ, followed by a dilation with the same transposed structuring element (a structuring element in mathematical morphology is a morphological elementary tool of a given simple geometry (circle, triangle, hexagon, bi-point, etc.) which is used to transform the image). It is defined by

$$g = f_{B(\lambda)} = ((f(x) \ominus \breve{B}(\lambda)) \oplus B(\lambda)). \tag{3}$$

The morphological closing corresponds to the reciprocal operation

$$g = f^{B(\lambda)} = ((f(x) \oplus \breve{B}(\lambda)) \ominus B(\lambda)). \tag{4}$$

These operators verify the properties of increasing and idempotence which are characteristic of morphological filters (see Appendix B). These filters are low-pass filters, but contrary to convolution products, they do not act by a symmetrical way on the image: openings (O) suppress the clear pics on an image (Fig. 1(c)), while closings (C) fill all the dark parts. From these basic elements, one can construct filters which correspond to opening and closing combination: in series (alternate sequential filters:

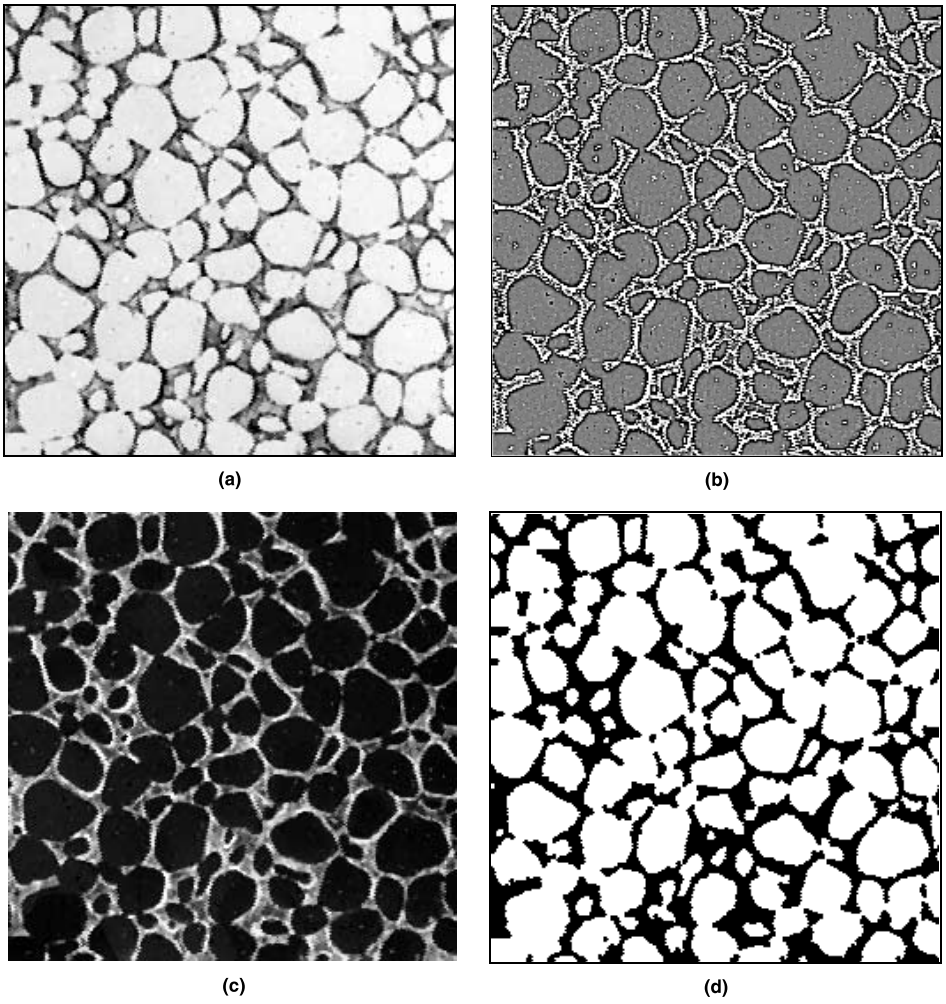

Fig. 2. (a) Effect of an order median filter, on image 1a. (b) Effect of a Laplacian filter, on image 2a. (c) Effect of a black top hat transformation of size 20 on image 2a. (d) Treatment of image 2c by a threshold between two grey tone levels (0–58) and binary morphology (erosion-reconstruction on two phases).

for example OCOC) or in parallel with sup and inf (morphological centres or morphological contrasts). At last a reconstruction can also be used (Fig. 1(a)), (see Appendix C).

Filters constructed from morphological residues correspond to high-pass filters of the linear domain. The morphological gradient [16] is defined by

$$g(x) = \mathrm{Mgrad}(f(x), B(\lambda)) = \frac{(f(x) \oplus \breve{B}(\lambda)) - (f(x) \ominus \breve{B}(\lambda))}{2\lambda}. \quad (5)$$

Another very useful morphological residue is the top-hat transformation [17]: it is made from the difference between the initial image and the opened image ("white hat") or between the closed and initial image ("black hat"), (Fig. 2(c)). The corresponding relationships are:

$$\mathrm{WTop\ hat}_{B(\lambda)}(f(x)) = f(x) - f_{B(\lambda)}(x), \quad (6)$$

$$\mathrm{BTop\ hat}^{B(\lambda)}(f(x)) = f^{B(\lambda)}(x) - f(x). \quad (7)$$

The top-hat transformation is also generalized in replacing simple openings by combined morphological filters.

6. Image segmentation

Attributes, which enable to define conditions of segmentation, can be related to textures, colours, grey tone levels or topography. They are associated either with the area itself or with its outline. In the first case one will speak of orientated region segmentation and in the second one of orientated contour segmentation.

6.1. Threshold

The threshold is the most simple and useful case of segmentation utilized in material science. If the case of colour images is, for instance, excluded, then threshold corresponds to the transformation of a grey tone image in a binary one. This step is extremely important as it corresponds to the maximum loss of information. Put simply, one can say that the file is eight times smaller. So one must pay a lot of attention to the choice of the method to be used. Two main categories can be defined:

- threshold from histogram in grey tone levels,
- threshold by contrast analysis.

The first category defines regions as a function of the grey tone level, and the second one mainly concerns the transition of grey tone levels on the outlines of the regions.

6.1.1. Threshold from grey tone level histogram

Several methods of threshold belong to this class.

6.1.1.1. Manual threshold or threshold by predefined levels. In this case the attribute of segmentation is a domain of grey tone level, defined by an upper and lower value. All image pixels with grey tones belonging to this domain will enable to create a binary image representing the set X which must be extracted. It can be defined by the following expression, where X is the union of the pixels of this attribute:

$$X = \{x : \max \geqslant f(x) \geqslant \min\}. \quad (8)$$

For a same image, several domains can be defined. A binary plane will correspond to each domain (Fig. 2(d)): that is the multiple threshold. The upper and lower thresholds can be defined by the operator or calculated from a threshold algorithm. In the following paragraphs, the most useful methods will be indicated, limiting ourselves only to the determination of a unique threshold (a multi-threshold is also possible, see Appendix D).

6.1.1.2. Threshold by maximization of the interclass variance. In this approach, the histogram is divided into a certain number of classes, P, being a priori a set. The relationship for two classes is given in Appendix D. When the position of the class limit varies, the value of the variance changes and the position(s) which maximize(s) that value is (are) determined. This type of threshold is sufficiently efficient when two classes are relatively more or less equivalent [18].

6.1.1.3. Threshold by entropy maximization. In this case the histogram is divided in several classes. The entropy is defined in Appendix D. This threshold by entropy maximization gives good results when there are few objects [19]. An example is given in [1].

6.1.1.4. Threshold by moment-preserving. The method proposed by Tsai [20] consists of assigning a well-determined grey tone level $z(j)$ to each class, so that the first statistical moments will be identical to that of the initial image. In the case of a system with two classes, one uses the three first moments as it is indicated in Appendix D. This method gives good results with low contrast images.

6.1.1.5. Threshold by contour information. The threshold by information on the contour is also possible from an algorithm computing the image contrast [21]. One considers two points x and y of the image and their grey tone level associated to $f(x)$ and $f(y)$. As one seeks for characterizing a contour, x and y will be all the close pixels of which the values are within the limits of the threshold t. They define a set $K(t)$ and the mean contrast for the threshold t is given by

$$\bar{C}(t) = \frac{\sum_{K(t)} \min(|f(x) - t|, |f(y) - t|)}{\mathrm{card}(K(t))}. \quad (9)$$

The threshold retained gives the maximum mean contrast. This type of threshold is efficient if the contours are related to only one transition, so to a two-phased system. An example is also given in [7].

6.2. Watershed: a segmentation by morphological operator

The watershed is the main segmentation method using morphological operators [16,22]. To describe how it works, one can imagine that a grey tone image can be assimilated to a relief. Any relief possesses lines of crests and catchment basins, i.e., zones for which the rain water flows towards a minima. These catchment basins are separated by a watershed line. The principle of construction is as follows: the low parts (minima) of the relief are filled (inundated) progressively but the lakes formed are prevented from joining by constructing a "dyke" which is nothing else than the watershed line. This construction method enables to classify the watershed among the geodesic operators (see Appendix C). All these operators use two source images to form segmentation: the minima which constitute the image of markers (Fig. 3(c)) and the reference geodesic image which represents the relief which will be inundated. In that example, the binary image (Fig. 3(a)) is converted into a grey tone image by the distance function (Fig. 3(b)). The quality of the segmentation will mainly depend on the choice of the markers. When the minima are directly used, it leads to an over-segmentation. To improve the result, extended minima will be utilized using either a sufficient depth in their neighbourhood (h min), (Fig. 3(c)) or minima brought together by dilation, or a combination of these two possibilities.

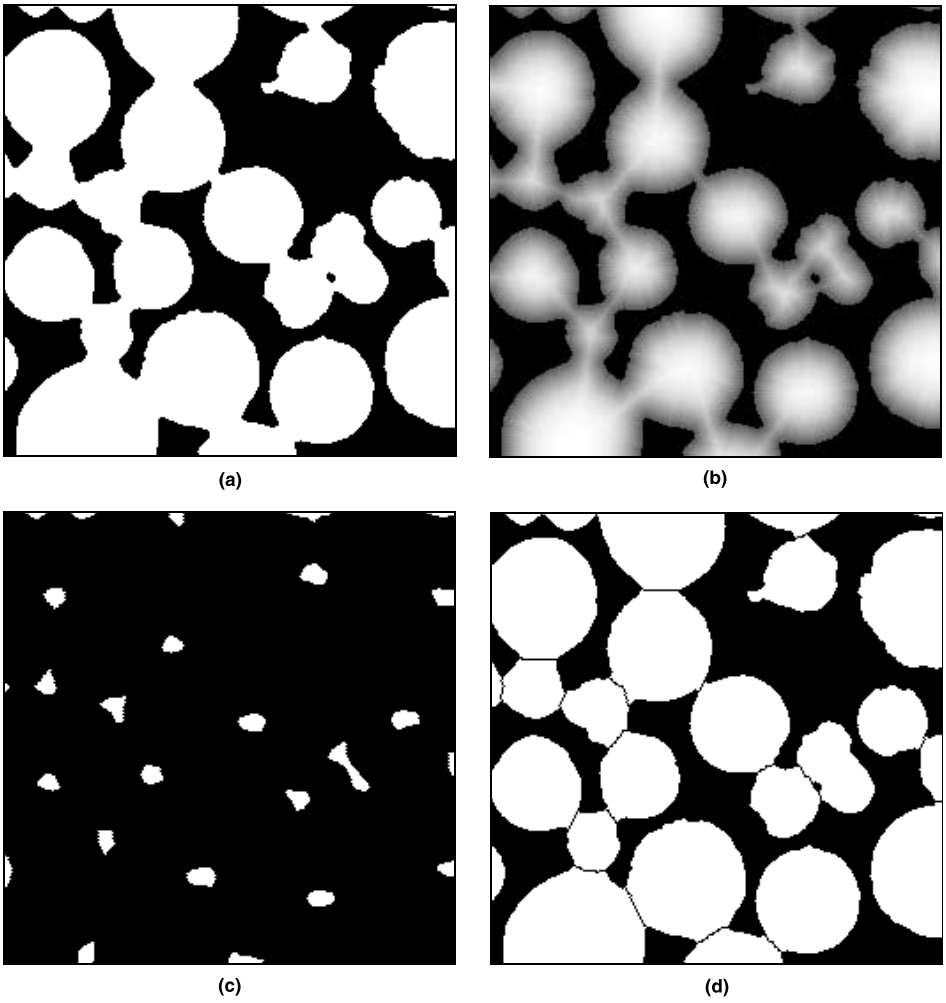

Fig. 3. (a) Binary image of a sintered glass. (b) Image of the distances to the border of the binary image 3a. (c) Binary image of dilated *h*-minima of image 3b (image of markers). (d) Result of the segmentation after application of the watershed method.

7. Binary image treatment

The watershed line and the segmentation by threshold give binary images which can operate as they are, but which can also require an image processing either by filtering or segmentation: it is often necessary to eliminate artefacts, to fill holes to separate objects which are touching, to extract useful information for the analysis. For this step, mathematical morphology [5,12] is a very powerful tool. The most often useful processing will then be presented.

7.1. Main operators

7.1.1. Binary filtering

Morphological filters used with images in grey tone levels have their equivalent in binary images (opening, closing, etc.). One has two main basic operators:

$$Y = X_{B(\lambda)} = ((X \ominus \breve{B}(\lambda)) \oplus B(\lambda)), \tag{10}$$

$$Y = X^{B(\lambda)} = ((X \oplus \breve{B}(\lambda)) \ominus B(\lambda)). \tag{11}$$

The morphological opening is most often replaced by the opening-reconstruction which has the advantage of not eliminating the smallest objects without modifying the remaining objects. For that purpose, the step of the Euclidean dilation is replaced by an infinite geodesic dilation of the eroded image (image of the markers) with regard to the initial image X:

$$Y = X_{X,B(\lambda)}((X \ominus \breve{B}(\lambda)) \oplus B_X(\infty)). \tag{12}$$

7.1.2. Elimination of the particles interesting the frame of measurements

When size distributions have to be performed particle per particle or when one has to investigate the shape of an object in 2D, that object must be totally included in the frame of measurements in order to avoid a bias. Mathematical morphology enables to rapidly eliminate objects intersecting that frame [5,12,23,24]. For that purpose one considers the image frame as a marker M and this frame is then reconstructed in the image X to be analysed. Objects totally included are obtained by the difference between the initial and reconstructed images:

$$Y = X/(M \oplus \breve{B}_X(\infty)). \tag{13}$$

7.1.3. Hole filling

In many cases, the result of segmentation leads to particles with holes, which has no physical meaning. Hence using geodesic operators of mathematical morphology, one must reconstruct the complementary of the objects to be analysed from the frame already used thus in inverting (reversing) the resultant image:

$$Y = (M \oplus \breve{B}_{X^C}(\infty))^C. \tag{14}$$

7.2. Other operators

These three previous operators constitute only a small fraction of the possibilities of mathematical morphology in segmentation. So it is not possible to give an exhaustive list. The skeleton $\mathrm{Sk}(X)$ and the skeleton by influence zone ($\mathrm{SKIZ}(X)$) are also often used.

7.2.1. Skeleton, Sk

If X is a connected set, δX its border and s a point of X, the skeleton X, noted $\mathrm{Sk}(X)$, is the union of the centre of the maximum balls included in X. Mathematically speaking it means

$$s \in \mathrm{Sk}(X) \iff \exists y_1, y_2 \in \partial X, y_1 \neq y_2 : \mathrm{d}(s, \partial X) = \mathrm{d}(s, y_1) = \mathrm{d}(s, y_2). \tag{15}$$

The skeleton by maximum disk (opened skeleton) is obtained from an algorithm developed by Lantuejoul [23]

$$\mathrm{Sk}(X) = \bigcup_{\lambda>0} \bigcap_{\mu>0} \Big((X \ominus \lambda\breve{B})/(X \ominus \lambda\breve{B})_{\mu B} \Big). \tag{16}$$

Nevertheless in the discrete space, this skeleton by opening is not topologically similar to the initial set. One prefers to often use the skeleton by thinning (see Appendix B) which leads to object of 1 pixel thickness and with the same topology. So it corresponds to a simplified representation of objects which can be used for a sorting. This skeleton possesses characteristic points: extremities and multiple points, which can present an interest, for example for branching information [25]. Nevertheless, one must pay attention to the use of the skeleton as it is sensitive to noise.

7.2.2. Skeleton by influence zone, SKIZ

The skeleton by influence zone (SKIZ) separates an image in several regions. Each region or influence zone, Y_i, is associated to an object X_i. It corresponds to the set of the nearest points of that object. Its mathematical definition is given by

$$Y_i = \bigcup (y : \mathrm{d}(y, x_i) < \mathrm{d}(y, x_j), x_i \in X_i \text{ and } x_j \in X_j). \tag{17}$$

The complementary set of these regions is the SKIZ:

$$\mathrm{SKIZ} = \left[\bigcup_i Y_i \right]^C. \tag{18}$$

For example, this operator is used to correctly represent the grain boundary network. It can also be used to investigate the neighbourhood of objects [24]: it can be very important to know, for example, the environment of certain crystals or cells in biology [26]. In fact it is the binary version of the watershed line.

An illustration of these different operators is given by the sequence of the images in Fig. 4.

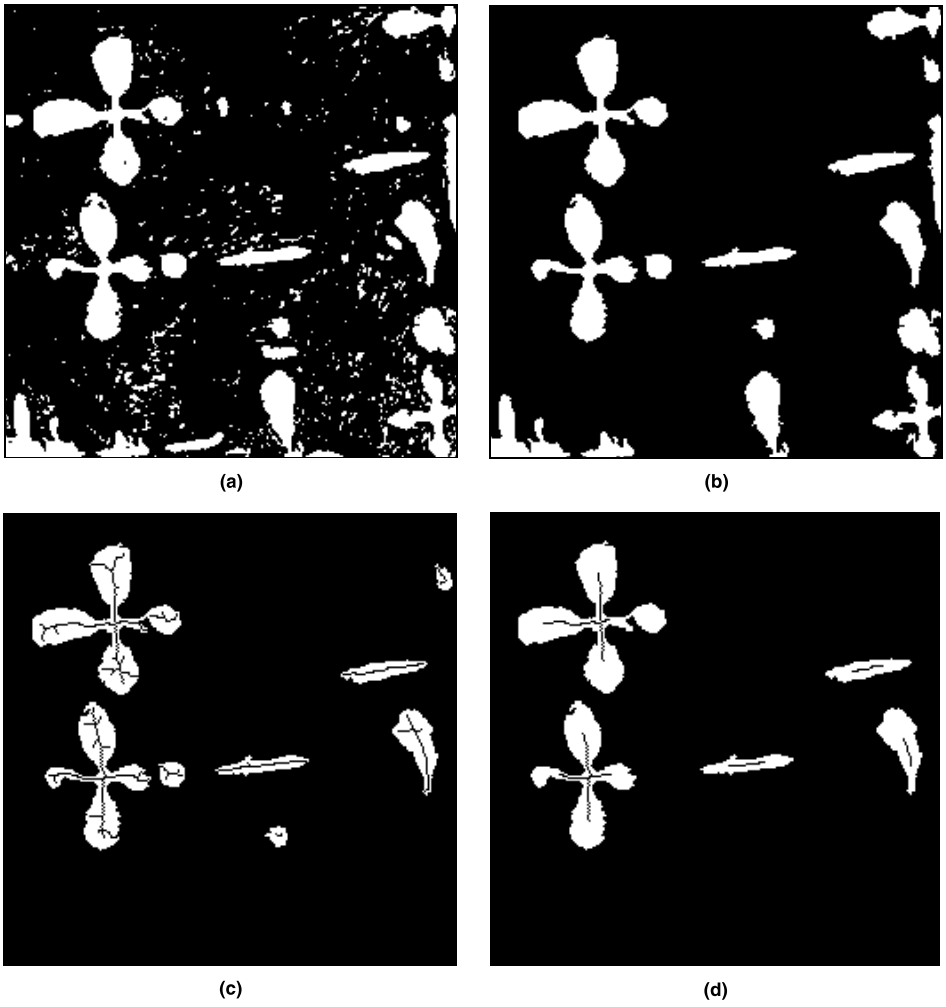

Fig. 4. (a) Threshold image of a cast iron. (b) Cleaned image by opening-reconstruction and hole filling. (c) Elimination of the particles intersecting the frame of measurements, and associated skeletons. (d) Clipped skeletons and particles reconstructed from markers.

Sorting of dendritic particles from others can be made by selecting the triple points of the pruned skeleton (centre of the skeleton cross of image 4d). Using these triple points as markers, only the dendrites are reconstructed.

To investigate cracks in concrete, it is necessary to use the skeleton function after their detection, as it can be seen in several papers of this issue [7,27,28].

7.3. Problem of local knowledge

As it has been already said, the structure of materials is always known in a frame of a size smaller than that of the plane section observed. The use of different operators of filtering or of segmentation introduces a bias on the borders of the image. To be rigorous one must eliminate certain zones as around the image. Mathematical morphology allows to solve this problem in defining the image zone (surface area) which is known without a bias. Hence, if one uses a local operator (morphological operator or convolution window (mask), the result will be known without bias in a frame Z' deduced from the initial frame (mask) by an operation of erosion with the structuring element B associated to the morphological operator or to the filtering function of the convolution product. This rule applies $Z' = Z \ominus B$ the theorem of the frame (mask) of measurements [12].

8. Measurements

After the segmentation and binary image processing, one can express the information contained in the image in parametric or function form. Characteristics related to objects or phases can be classified according to several criteria: ratio, size, shape and dispersion of the phases. The partial knowledge of a 3D structure through

a part of a 2D section introduces constraints on the choice of the parameters when one wishes to access 3D space. In this case parameters or functions only with stereological properties must be used.

8.1. Stereological parameters

The stereological parameters [3–5] verify a certain number of properties, as proposed by Hadwiger [29] in the case of sets corresponding to a finite union of convex bodies. These properties can easily be explained, particularly in the case of stationary systems.

If $W(X)$ is a measurement on the set X, this measurement must not depend on the position of X. One says that $W(X)$ is invariant under translations and rotations.

As any optical system enables one to obtain images of various magnifications, the measurement must not depend on the magnification. It is then said that the measurement is compatible with similarities.

Although any experimentalist would try to work on the clean image, residual noise remains. So the measurement must mathematically be robust. That can be guaranteed if the measurement verifies the property of continuity. The stability will still be possible if the measurement is upper semi-continuous or lower semi-continuous.

As the measurement is made only on a part of the set, the magnitudes will be estimated by means, and consequently by sums. In the case of sets, the measurement will verify the C-additivity. This last property is a limiting condition. So it can be shown that a numbering of objects does not correspond to a C-additive measurement.

In the case of a stationary system and to be independent on the size of the frame of measurements, the measurements will be given as a function of the frame size of the defined space: this will be termed local parameters opposed to global or absolute parameters.

In the space with n dimensions, there only exist $n+1$ basic parameters, which verify these properties. They are gathered in Table 1. Some remarks can be made.

The norm (integral of mean curvature in $\mathbb{R}^2$) is generally called integral of mean curvature. To each point of the boundary corresponds two main curvatures. If these two curvatures are positive, the surface is convex. If they are negative, the surface is concave. If the main curvature is positive and the other one negative, one has a surface like a saddle: then for each point one can define a mean curvature which is integrated to obtain the norm.

The specific connectivity numbers in $\mathbb{R}^3$, $\mathbb{R}^2$ and $\mathbb{R}^1$ are the Euler–Poincaré characteristics (EPC), [12,30]. In $\mathbb{R}^1$ it corresponds to the number of segments per unit length, intersected by a straight line Δ on the object X. In $\mathbb{R}^2$ it corresponds to the number of objects less the number of holes contained in these objects per unit surface. In $\mathbb{R}^3$, it is more complicated as this number is calculated from the topological nature of surfaces making the objects (number minus genus).

There exist stereometric relationships between the parameters of a same column [3–5]. For a stationary set, there is:

$$V_V(X) = A_A(X) = L_L(X) = P_P(X), \tag{19}$$

$$S_V(X) = 4N_L(X), \quad L_A(X) = \pi N_L(X), \tag{20}$$

$$M_V(X) = 2\pi N_A(X). \tag{21}$$

One notes that the Euler–Poincaré characteristics are only accessible in their own space. From these basic parameters, secondary parameters, which verify the same properties, can be defined. The most used parameters are related to the size: there are the mean free path, $L_1(X)$, and the mean surface area of objects without holes, $\bar{A}(X_i)$. They are calculated from

$$L_1(X) = \frac{V_V(X)}{N_L(X)} \quad \text{and} \quad \bar{A}(X_i) = \frac{V_V(X)}{N_A(X)}. \tag{22}$$

Table 1
Stereological parameters in the local case

Space	Parameters of quality	Measure of boundary	Measure of curvature	
$\mathbb{R}^3$	Volume fraction	Specific surface area	Specific norm	Specific connectivity number
	$V_V(X)$	$S_V(X)$	$M_V(X)$	$N_V(X)$
$\mathbb{R}^2$	Surface fraction	Specific perimeter	Specific connectivity number	
	$A_A(X)$	$L_A(X)$	$N_A(X)$	
$\mathbb{R}^1$	Linear fraction	Specific connectivity number		
	$L_L(X)$	$N_L(X)$		
$\mathbb{R}^0$	Point fraction $P_P(X)$			

It is also to be noted that the measure of $N_L(X)$ is a function of the orientation of the analysis straight line Δ. Several examples are given in this issue and more particularly in [7,31].

8.2. Stereological parameters and frame of measurements

The problems of local knowledge also exist in the case of stereological measurements. Two approaches are possible to obtain results without a bias. In the first case, one can consider that the measurement is associated to a hit or miss transformation. In these conditions, the theorem of the frame of measurements will also be applied. In the second case, one will use the notion of shell [32]. For a measurement of the connectivity number, $N_2(X)$, the shell Q will be made of two adjacent sides of the rectangular mask Z. The non-biased value of $N_A(X)$ will be given by

$$N_A(X) = \frac{N_2((X \cap Z) \cup Q) - 1}{A(Z)}. \tag{23}$$

In the case of the connectivity number $N_L(X)$, the frame of measurements Z' is a segment of line $(\Delta \cap Z)$ and the shell Q' is one of the extremities of this segment. The non-biased measurement is given by

$$N_L(X) = \frac{N_1((X \cap Z') \cup Q) - 1}{L(Z')}. \tag{24}$$

8.3. Parameters related to individual analysis

When the phase X corresponds to many objects isolated one from the others, measures of size (Feret diameters, etc.), of shape (as the ratio length/thickness or surface/(perimeter^2), etc., can be performed [3–5]. But all these parameters do not possess any stereological character, which limits their use only to a comparison and not to an estimation of some 3D characteristics of the material.

8.4. Morphological functions

The mean stereological parameters are often insufficient to access a precise evaluation of the morphological characteristics. Thus very different structures can give the same value of the mean free path. So a more accurate description can be obtained using functions depending on a parameter.

One can distinguish:

- the granulometric distribution functions to characterize the size,
- the covariance functions to characterize the phase dispersion,
- the distance functions to also characterize the phase dispersion but by another approach,
- the rose of intercepts or of directions to characterize the structure anisotropy.

8.4.1. Granulometric functions

Granulometric functions are the most useful. To undertake granulometric measures, there exists two main categories of methods: measurement by individual analysis or by morphological opening.

8.4.1.1. Individual granulometric analysis. Individual granulometric analysis is very well known: the size of each object is measured. Then they are classified according to their size to establish the distribution. To perform such an analysis, each object must be totally visible. So one is constrained to eliminate objects intersecting the frame of measurements, which introduces a bias as the largest objects are (most often) eliminated from the measure. To correct this bias, one assigns to the counting a coefficient which is nothing else than the reciprocal probability of inclusion of the object in the frame. This probability is easily obtained from the ratio surface area of the frame of measurements Z/rectangle to the object [24]. An example is given in [6].

8.4.1.2. Opening granulometry. The granulometric analysis by opening is a more general method than the previous one, as it can be used independently on the nature of the set X. The granulometric distribution in measure is given by

$$G(\lambda) = \frac{A_A(X \cap (Z \ominus B(2\lambda))) - A_A(X_{B(\lambda)} \cap (Z \ominus B(2\lambda)))}{A_A(X \cap (Z \ominus B(2\lambda)))} \tag{25}$$

$B(\lambda))$ is a convex structuring element of size λ. It can be a square, an hexagon, a segment, etc. It can also be performed on grey tone images (Fig. 5(a) and (b)). In this case, the measurement is made on the volume under the image, which replaces the surface fraction. The use of a linear structuring element, ℓ, leads to linear granulometries which are particularly interesting as the estimate in $\mathbb{R}^2$ remains valid for $\mathbb{R}^3$ [33,34]. Of course erosion by a segment is sensitive to the orientation α of the segment ℓ. That will be useful to make estimates on the structure anisotropy. One can obtain granulometry in number and in measure directly from the erosion which gives the function $P(\ell)$, (probability that a segment ℓ is included in the objects). One has

$$P(\ell) = A_A((X \ominus \ell) \cap (Z \ominus \ell)). \tag{26}$$

It induces

$$G(\ell) = \frac{P(0) - P(\ell) + \ell P'(\ell)}{P(0)}$$

for granulometry in measure, (27)

$$F(\ell) = \frac{P'(0) - P'(\ell)}{P'(0)}$$

for granulometry in weight. (28)

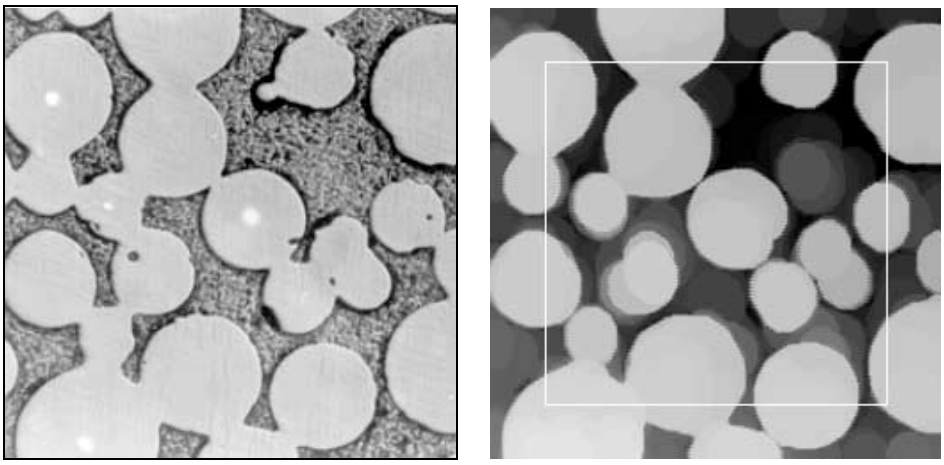

Fig. 5. (a) Image of a sintered glass. (b) Opening of size 30 on image 5a and mask Z' inside of which the result is known without bias.

By integration of the $P(\ell)$ function one obtains the star function in $\mathbb{R}^3$ which corresponds to the mean volume of the set X seen from any point of X. One has

$$St_3(X) = \frac{4}{P(0)} \int_0^\infty \ell^2 P(\ell) \mathrm{d}\ell. \tag{29}$$

8.4.2. Covariance function and dispersion

The covariance function is obtained by erosion of the analysed structure by a bi-point h. One distinguishes the (simple) covariance, for which two points at distant h are tested on the same phase, X, and the crossed or rectangular covariance for which each point belongs to different phases, X and Y.

8.4.2.1. Simple covariance. The simple covariance is given by

$$\begin{aligned} C(h) &= A_A((X \ominus h) \cap (Z \ominus h)) \\ &= A_A((X \cap X_{\vec{h}}) \cap (Z \cap Z_{\vec{h}})). \end{aligned} \tag{30}$$

To obtain a measure of covariance, it is simpler to take the intersection of X and of its translated by $\vec{h}$. The value at the origin is nothing else than $A_A(X)$. The slope is equal to $N_L(X)$. For $h \to \infty$ the covariance tends towards a horizontal asymptote equal to $A_A(X)^2$. Between the origin and the value at the infinite, the behaviour of the covariance is related to the state of dispersion of the phase X. Perfectly random structures without attraction or repulsion effect will give a regularly decreasing curve. A repulsion effect between the different parts of X will give a curve passing below the asymptote, while with an attraction case it passes above. For a periodic structure the $C(h)$ curve will oscillate. As for the $P(\ell)$ function, the covariance function is a directional analysis related to the orientation of $\vec{h}$.

8.4.2.2. Crossed covariance. The crossed or rectangular covariance corresponds to

$$C(X/Y, h) = A_A((X \cap Y_{\vec{h}}) \cap (Z \cap Z_{\vec{h}})). \tag{31}$$

The rectangular covariance enables to investigate the dispersion of phase X with regard to Y in polyphased systems. But in this case the asymptote corresponds to $A_A(X) * A_A(Y)$, while the value at the origin is null and the slope is equal to $1/4S_V(X, Y)$. It has been used by several authors of this issue [1,7,31].

8.4.3. Distance functions and dispersion

A more physical approach of the dispersion uses the distance function. Several distance functions can be defined. The three main functions are described in this issue: the distance between the nearest neighbours, the mean distance between neighbours, and the distance function for which the value of each pixel is given by its distance to the phase under investigation [35]. This type of characterization is very important for materials of civil engineering and gives rise to European and American standards and to many papers ([35,36]).

8.4.4. Rose and anisotropy

Anisotropy investigation can be performed using analysis tools sensitive to orientation. If $N_L(X, \alpha)$ is a function, as it corresponds to diametral variation in the direction α, this value can be plotted in polar coordinates as a function of α; thus the rose of intercepts can be constructed [4,5]. One example derived from this method is given in [37].

The rose of intercepts is particularly useful when there is one dominant orientation. When there are several directions, it is better to use the rose of directions which corresponds to the ratio of length of boundaries

orientated in a given direction [4,5]. An example is also given in [7].

Unfortunately numerical images do not lend themselves to an angular investigation as it is difficult to convert an image into a square or hexagonal grid according to any angle without using interpolations which can induce errors. The ideal is to have a rotating optical or captor device.

9. Modelling

As it has been indicated a structure of a material can only be characterized by a large number of parameters or functions. Moreover, the majority of these parametric characterizations are not of stereological nature. So the modelling of a structure, in favourable cases, can solve that problem.

To model a structure, several strategies are at our disposal: (i) either one can use the physical process of formation of the structure or associated to a physical behaviour, (ii) or use probabilistic models as Boolean models. The first strategy is illustrated here by the paper of Boussa et al. [38], while the second one corresponds to the works of Dequiedt et al. [39] and Jeulin et al. [40]. In the following only the second strategy will be approached.

To observe a morphology, it requires that the set X does not fill all the space. So there will be at least a medium of two components: a set X and its complementary X^{C}. Objects constituting that set can be as well points than straight lines or any sub-sets. The obtained set will be a random topologically closed set (random closed set, RACS), [15,41–44]. This restriction is necessary to preserve good properties, but it is not in practice inconvenient. Thus a RACS will remain a RACS after an erosion, a dilation.

The choice of a model depends on a certain number of prior knowledge. In the case of bulk materials, the number of morphologically discernable phases is the first element. So there will be two main categories: monophased materials, which will be described from a space tessellation, and polyphased materials described from polyphased RACSs. Inside these categories other elements must be taken into consideration such as shape, dispersion, size distribution, etc.

9.1. Choquet's capacity

A RACS can be characterized by a probability of events corresponding to morphological measurements such as the probability of inclusion of a compact K in a set or its complementary. That is the role attributed to the Choquet's capacity, $T(K)$, defined by [41,45]

$$T(K) = \Pr(X \cap K \neq \emptyset). \tag{32}$$

One also can define $T(K)$ from the probability $Q(K)$ that the intersection between X and K is empty:

$$Q(K) = 1 - T(K) = \Pr(X \cap K = \emptyset) = \Pr(K \subset X^{C}). \tag{33}$$

As a distribution function defines a random variable, the knowledge of the Choquet's capacity for a compact K enables to completely define a probabilistic model. It is evident that all the possible compacts cannot be tested. One will use the simplest ones: the segment of line (the more isotropic (hexagon or square) structuring element), ℓ, the bi-point, h, through the covariance. It can be seen from Eq. (33) that the Choquet's capacity could be tested in using only operations of erosion on the considered compact.

9.2. Point Poisson process

The starting point of all probabilistic models is the point Poisson process. The probability that n points of a Poisson process of density θ belong to a set Z is given by

$$\Pr(Z) = \frac{(\theta \operatorname{mes}(Z))^{n}}{n!} \exp(-\theta \operatorname{mes}(Z)). \tag{34}$$

This point process is the basis of all derived models such as clusters or hard core models [46].

9.3. Classification of probabilistic models

The probabilistic models can be classified into several categories:

- tessellation models,
- polyphased models.

9.3.1. Tessellation models

9.3.1.1. Voronoi tessellation. The most known tessellation is that of Voronoi. To construct it, one sets points p_i according to a Poisson process of density θ. To each point p_i corresponds an influence zone X_i defined by

$$X_i = \{x : d(x, p_i) < d(x, p_{j \neq i})\}, \tag{35}$$

where $d(x, p)$ is the distance from x to p. This influence zone is a convex polygon in $\mathbb{R}^2$ and a convex polyhedron in $\mathbb{R}^3$. Fig. 6 illustrates such a model. There also exists other models such as the Poisson tessellation or the Johnson–Mehl [47] model which subdivide the space. Among those, only the Poisson tessellation possesses a stereological character and is easy to test from the Choquet's capacity.

9.3.1.2. Poisson tessellation. The space tessellation in $\mathbb{R}^2$ according to a Poisson process is made from Poisson straight lines [48]. They are constructed as follows. If Δ

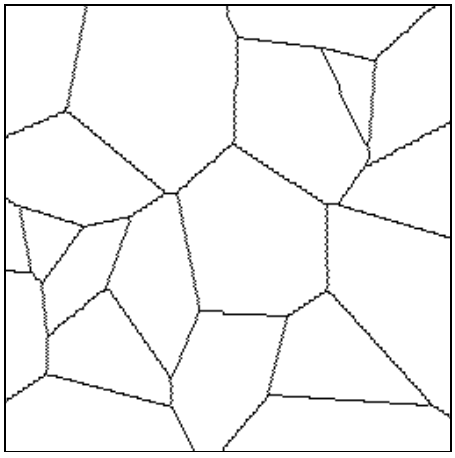

Fig. 6. Voronoi tessellation in $\mathbb{R}^2$.

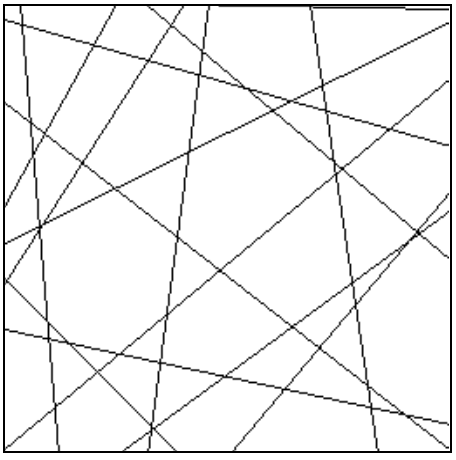

Fig. 7. Poisson mosaic.

is a straight line with an orientation between ω and $\omega + d\omega$ and passing through the origin of the plane, on that straight line one realizes a point Poisson process of density $\lambda_2 d\omega$. To each point one sets a Poisson straight line perpendicular to Δ. In the case of an isotropic mosaic, λ is constant and the value of ω is chosen according to a uniform law of probability. The $\mathbb{R}^2$ space is then divided into an infinite number of random polygons called Poisson polygons (Fig. 7).

9.3.2. Polyphased models

The most known two-phased RACS model is the Boolean model [49]. To each point of the Poisson process of density θ, a primary grain is set. The Boolean model is the union of all these primary grains. The main morphology will largely depend on these primary grains which opens up many possibilities (Fig. 8(a) and (b)). The Boolean scheme models the same properties in a sub-space (stereological characteristic). Moreover, if X' is a primary grain of the Boolean scheme, one has

$$Q(K) = \exp(-\theta E(\mathrm{mes}(X' \oplus \bar{K}))). \tag{36}$$

Thus it is easy to test it by the Choquet's capacity.

Other polyphased models exist, but they are beyond the scope of this general paper [44]. One can quote, for example, dead leave models [50] and Stienen's model [51].

10. Concluding remarks

The scope of this paper was to give a short overview of automatic image analysis, and on mathematical morphology, in order to facilitate a better understanding of the papers included in this special issue on the use of that technique in the field of civil engineering materials.

Other more detailed and complementary information can be found in the main books related to this subject [3–5,12,14,52–64].

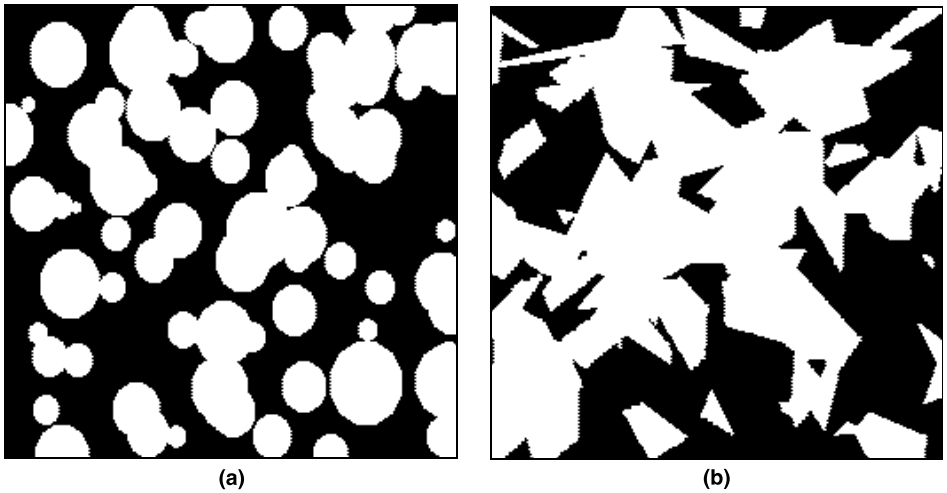

Fig. 8. (a) Boolean model with circular disks of normal distribution. (b) Boolean model with Poisson grains.

Acknowledgements

This work has been performed in the frame of the "Pôle Traitement et Analyse d'Images" of Basse-Normandie (Pôle TAI): Image Processing and Analysis Pôle of Basse-Normandie.

Appendix A. Definition of images

Images are defined by two main characteristics:

- a support belonging to the metric space of a given dimension (generally 2, sometimes 3),
- one or several functions.

If x is a point of the support Z, the functions associated to this point will be defined by $Fi(x)$. When the images have to be processed on a computer, the support is represented by a grid of points regularly spaced. In $\mathbb{R}^2$ these points are distributed according to a square or hexagonal grid. In $\mathbb{R}^3$ one generally uses a cubic grid. So the numerical supports are represented by n lines and m columns. That gives the dimension of the image. The most common values today are 256×256 and 512×512.

The functions associated to each point are themselves extended to numbers. Then different types of images must be distinguished:

- binary images, related to sets where $f(x)$ takes either the value 1 if the point belongs to the set, or 0 if not,
- grey tone images, which can be most often coded on 8 bits (black = 0 and white = 255); one can also use integer on 16 bits or real numbers,
- multimodal and colour images where each mode or each primary colour will be represented by a grey tone image.

At that level, multimodal images must be distinguished from colour ones. For multimodal images the different modes are independent. For colour images the primary colour defines a vectorial space. The most common mode of vectorial representation is the mode RGB (red, green, blue). Nevertheless other representations also exist. The mode HSL, where the primary colours are replaced by hue, saturation and luminance. The mode YIQ is characteristic of the American television standard (Y: luminance component; I and Q: chrominance components).

The filtering of colour images by operators without good vectorial properties leads to a problem. That is the case of many filters. Hopefully with image analysis, one does not try to reconstruct the filtered colour image, but to treat separately each plane to extract the pertinent information.

Taking into account the real nature of materials in civil engineering, one has to use sometimes such images.

Appendix B. Elements of mathematical morphology

Examples given to illustrate mathematical morphology will only concern binary images. The approach to functions is made via the sub-graph. All the morphological operators are based on the notion of structuring element, noted B_x, when it is located in a point x of an image.

Erosion. The eroded of the set X is a set of points x of the image such as B_x is totally included in X. It is written as

$$X \ominus \breve{B} = \{x : B_x \subset X\}. \tag{B.1}$$

Fig. 9 presents an example of erosion by an hexagon. The small details (smaller than the size of B_x) disappear. In the case of images in grey tone levels, the definition of the erosion by a flat structuring element attributes to a current pixel the smallest value of pixels in the domain defined by the structuring element. One has

$$g(x) = f(x) \ominus \breve{B} = \inf(f(y) : y \in B_x). \tag{B.2}$$

Dilation. Dilation is the dual operation of erosion with regard to the complementation. It is the set of points x such as B_x has a not-empty intersection with X. It is written as

$$X \oplus \breve{B} = \{x : B_x \cap X \neq \emptyset\}. \tag{B.3}$$

Fig. 10 illustrates this operator. Near objects are connected and holes filled. In the case of images in grey tone levels, the definition of dilation by a flat structuring element attributes to a current pixel the highest value of pixels of the domain defined by the structuring element. One has

$$g(x) = f(x) \oplus \breve{B} = \sup(f(y) : y \in B_x). \tag{B.4}$$

As it was indicated earlier the opening and closing operators can immediately be deduced (see Fig. 11).

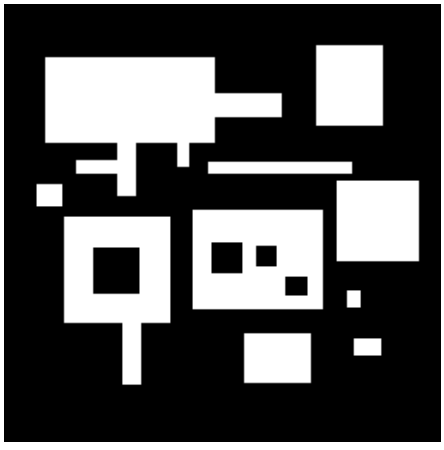

Fig. 9. Initial image.

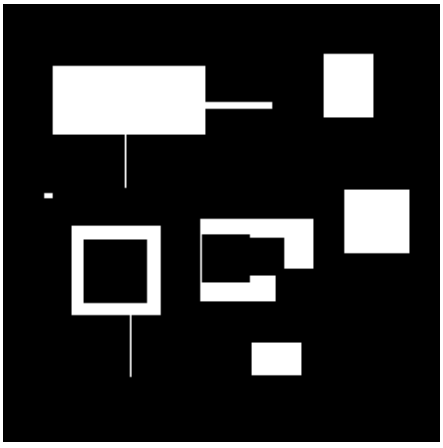

Fig. 10. Erosion by a square of size 5 on image Fig. 9.

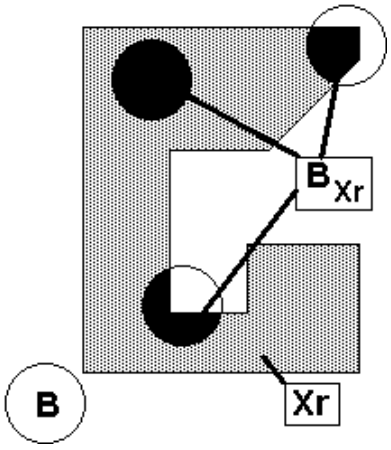

Fig. 12. Comparison between Euclidean disk and geodesic disk with a set *Xr* as reference.

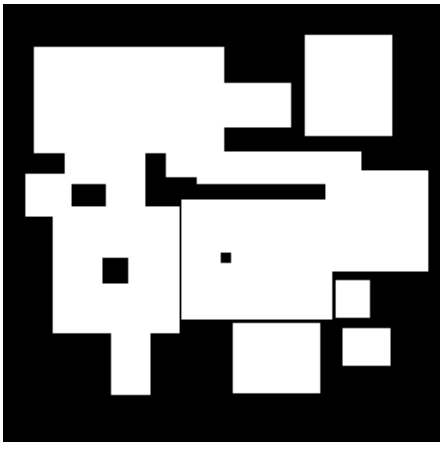

Fig. 11. Dilation of a square of size 6 on image Fig. 9.

Fig. 13. Initial sets. Reference set *Xr* is in grey, *Y* set in white.

Hit or miss transformation. The hit or miss transformation is more general. The structural element B is constituted of two sub-elements $T_x(a)$ and $T_x(b)$, respectively, related to X and X^C. The point x will be at 1 if $T_x(a)$ is included in X and if $T_x(b)$ is included in X^C. One has

$$X \circledast B = \{x : (T_x(a) \subset X) \text{ and } (T_x(b) \subset X^C)\}. \quad \text{(B.5)}$$

These operators are used to extract particular points such as extremities and multiple points of the skeleton. They are also used with thinning and thickening operators.

Thinning. The thinning operation consists of suppressing points of an object having a given neighbourhood configuration. It is defined by the following operator:

$$X \bigcirc B = X/(X \circledast B). \quad \text{(B.6)}$$

It is used to obtain homotopic skeleton and the centres of objects.

Thickening. Thickening is the dual operation of thinning: one adds to the object the points having a given neighbourhood configuration. It is defined by the following operator:

$$X \odot B = X \cup (X \circledast B). \quad \text{(B.7)}$$

It is used to have the skeleton by influence zone or to obtain a convex hull. The thinning and thickening operations defined for binary images have their equivalent in grey tone images.

Appendix C. Geodesic operators

Erosion and dilation defined in Appendix B were performed in the Euclidean space. The square structuring element used is the extension in the digital space Z^2 of the circular disk B of size λ defined in $\mathbb{R}^2$. If B is

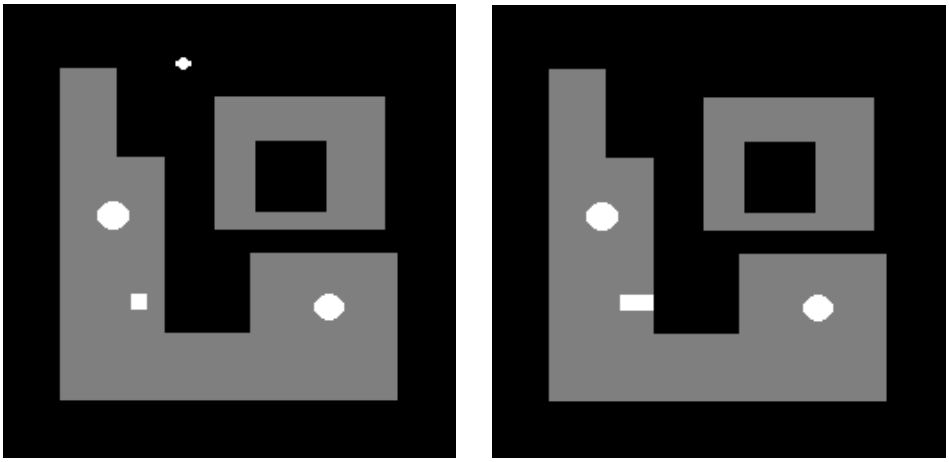

Fig. 14. (a) Euclidean erosion of the set Y by an hexagon of size 10. (b) Geodesic erosion of the set Y by an hexagon of size 10.

centred on x, then the corresponding closed disk or ball is defined by

$$B_x = \{y : d(x,y)\lambda\}. \tag{C.1}$$

$d(x,y)$ is the Euclidean distance between x and y, and B a Euclidean disk (in $\mathbb{R}^2$) or ball (in $\mathbb{R}^3$).

Geodesic erosion and dilation are performed with geodesic disks or balls for which the notion of Euclidean distance is replaced by the geodesic distance one. The geodesic distance is defined with regard to a reference set, noted Xr. In the case of the geodesic distance the shortest way to go from one point x to a point y is not the segment $\overline{xy}$, but an arc $\overset{\frown}{xy}$ totally included in Xr. There exists properties associated with the notion of distance, such as the triangular inequality. There also exists in the frame of the geodesic distance, but one adds the following property: if the path between point x and point y is not totally included in Xr, then $d(xy)$ has an infinite value. Fig. 12 presents how a disk B can be modified with regard to the reference set (see Fig. 13).

The definitions concerning erosion and dilation practically remain the same for the corresponding geodesic operations. One only has to replace the Euclidean disk or ball by a geodesic one:

$$Y \ominus \breve{B}_{Xr} = \{x : (B_{Xr})_x \subset Y\}, \tag{C.2}$$

$$Y \oplus \breve{B}_{Xr} = \{x : (B_{Xr})_x \cap Y \neq \emptyset\}. \tag{C.3}$$

Figs. 14 and 15 illustrate the effects of erosion and dilation of a set Y with regard to the set Xr (Fig. 13). One notes that the border of the set Y is not affected by the erosion and dilation operations when it is common to Xr.

The main application of the geodesic operation on sets is the reconstruction. To define a reconstruction

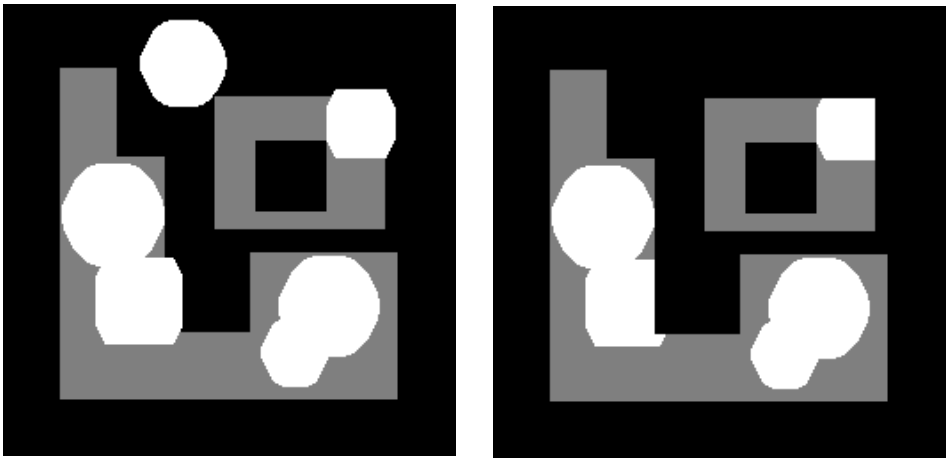

Fig. 15. (a) Euclidean dilation of the set Y by an hexagon of size 10. (b) Geodesic dilation of the set Y by an hexagon of size 10.

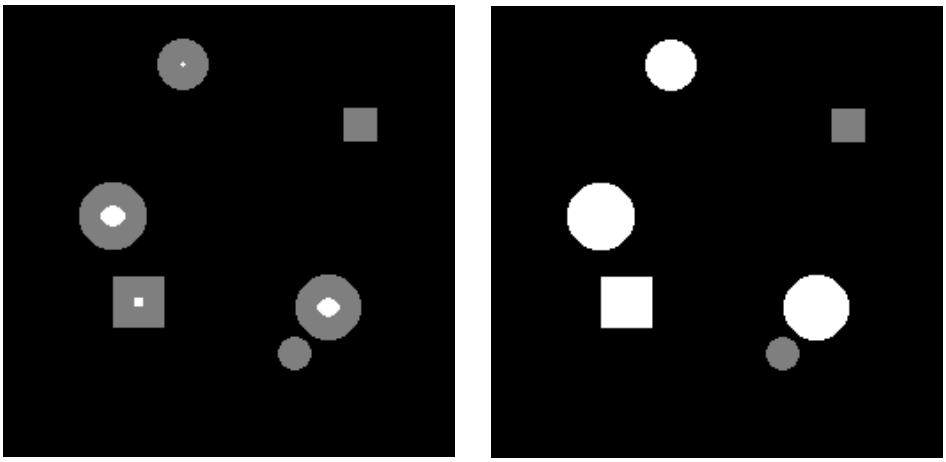

Fig. 16. (a): Erosion (in white) of size 12 on the Y set (in grey) to obtain markers for reconstruction. (b) Result of opening by reconstruction (in white).

operation one must have a reference Xr in which the set Y will be reconstructed by a geodesic dilation of infinite size. It is written as

$$\text{Build } (Y : Xr) = Y \oplus \breve{B}(\infty)_{Xr} = (Y \oplus \breve{B}(1) \cap Xr)_{n=\infty}. \tag{C.4}$$

So it can be obtained from a dilation of size 1 followed by an intersection by Xr. The process is iterated until idempotence, i.e., until the image remains unchanged.

This operator will be found in the case of hole filling, of the elimination of particles intersecting the frame of measurements, and with the opening operator by reconstruction.

Fig. 16 illustrates this operator.

Appendix D. Threshold and data analysis

Parameter	*Meaning*
m	maximum value of the grey tone levels
M_k	moment of order k of an image ($k = 1$: mean)
N	number of pixels of an image
$n(i)$	number of pixels with a grey level i
t	threshold to determine
$C(1)$	class of pixels with grey tone levels between 0 and t
$C(2)$	class of pixels with grey tone levels between $t+1$ and m
$N(1)$, $N(2)$	number of pixels of the class $C(1)$, $C(2)$
$M_1(1)$, $M_1(2)$	mean of pixels of the class $C(1)$ and $C(2)$

Entropy for two classes:

$$H(t) = H(C(1)) + H(C(2)) = -\sum_{i=0}^{t} \frac{n(i)}{N(1)} \ln\left(\frac{n(i)}{N(1)}\right) - \sum_{i=t+1}^{m} \frac{n(i)}{N(2)} \ln\left(\frac{n(i)}{N(2)}\right).$$

Interclass variance for two classes:

$$V(t) = (M_1(1) - M_1)^2 \frac{\sum_{i=0}^{t} n(i)}{N(1)} + (M_1(2) - M_1)^2 \times \frac{\sum_{i=t+1}^{m} n(i)}{N(2)}.$$

System of equations for the moment conservation:

$$M_k = \frac{\sum_{i=0}^{t} n(i)}{N(1)} z(1)^k + \frac{\sum_{i=t+1}^{m} n(i)}{N(2)} z(2)^k.$$

References

[1] Ringot E, Bascoul A, Mowret M. Image analysis: at tool for the characterization of hydration of cement in concrete-metrological aspects of magnification on measurement. Cem Concr Comp 2001;23:201–6.
[2] Matheron G. Les variables régionalisées et leur estimation. Paris: Masson; 1965.
[3] DeHoff RT, Rhines FN. Quantitative microscopy. New York: McGraw-Hill; 1968.
[4] Underwood EE. Quantitative stereology. Reading, MA: Addison-Wesley; 1970.
[5] Coster M, Chermant JL. Précis d'analyse d'images. Paris: Les Editions du CNRS; 2nd ed. Paris: Les Presses du CNRS, 1989.
[6] Redon C, Chermant L, Coster M, Chermant JL. Measurements of orientation in discretized space by Fourier transform: automatic investigation of fiber orientation in a reinforced concrete. Acta Stereol 1998;17:93–8.

[7] Chermant JL, Chermant L, Coster M, Dequiedt AS, Redon C. Some fields of applications of automatic image analysis in civil engineering. Cem Concr Comp 2001;23:157–69.
[8] Slate FO, Olsefski S. X-rays for study of internal structure and microcracking of concrete. J Am Concr Inst 1963;(May): 575–88.
[9] Bentz DP, Martys NS, Stutzman P, Levenson MS, Garbozi EJ, Dunsmuir J, Schwartz LM. X-rays microtomography of an ASTM C109 mortar exposed to sulfate attack. Mater Res Soc Symp Proc 1995;370:77–82.
[10] Quenec'h JL, Jeulin D, Coster M, Chermant JL. Approach of liquid phase sintering process by probabilistic models. In: Jeulin D, editor. Advances in theory and applications of random sets. Singapore: World Scientific; 1997. p. 231–49.
[11] Pratt WK. Digital image processing. New York: Wiley; 1991.
[12] Serra J. Image analysis and mathematical morphology. London: Academic Press; 1982.
[13] Chermant JL, Coster M. Role of mathematical morphology in filtering, segmentation and analysis. Acta Stereol 1994;13:125–36.
[14] Serra J. In: Serra J, editor. Image analysis and mathematical morphology, vol 2: Theoretical advances. London: Academic Press; 1988 [chapter 5].
[15] Serra J. Mathematical morphology course. Paris: Ecole des Mines de Paris; 1998.
[16] Beucher S. Segmentation d'image et morphologie mathématique. Thèse de Docteur-Ingénieur. Paris: Ecole des Mines de Paris; 1990.
[17] Meyer F. Contrast feature extraction. In: Chermant JL, editor. Quantitative analysis of microstructures in materials science, biology and medecine, Pract Met 1978;S8:374–80.
[18] Otsu N. A threshold selection method from gray-level histogram. IEEE Trans Syst Man Cybernet 1979;9:62–6.
[19] Kapur JN, Sahoo DK, Wong AKC. A new method for gray-level picture thresholding using the entropy of the histogram. Comp Vision Graph Image Process 1985;29:273–89.
[20] Tsai W.-H. Moment-preserving thresholding: a new approach. Comp Vision Graph Image Process 1985;29:377–93.
[21] Kohler R. A segmentation system based on thresholding. Comp Vision Graph Image Process 1981;15:319–38.
[22] Meyer F, Beucher S. Morphological segmentation. J Visual Comp Image Represent 1990;1/1:21–46.
[23] Lantuejoul C. La squelettisation et son application aux mesures topologiques des mosaïques polycristallines. Thèse de Doctorat of the Ecole des Mines de Paris; 1978.
[24] Lantuejoul C. On the estimation of mean values in individual analysis of particles. Microscopica Acta 1980;5:266–73.
[25] Coster M, Chermant L, Chermant JL. Separation of different shapes by sequential image transformation. Stereol Iugosl 1981;3(Suppl):175–83.
[26] Herlicoviez D, Chermant L, Coster M, Chermant JL. Contribution of image analysis to a study of muscle changes in hypothyroïd rats. Acta Stereol 1983;2:107–12.
[27] Ringot E, Bascoul A. About the analysis of microcracking in concrete. Cem Concr Comp 2001;23:261–6.
[28] Ammouche A, Riss J, Breysse D, Marchand J. Image analysis for automatic study of microcracks in concrete. Cem Concr Comp 2001;23:267–78.
[29] Hadwiger H. Vorslesungen über inhalt, oberfläche und isoperimetrie. Berlin: Springer; 1957.
[30] Nagel W, Ohser J, Pischang K. An integral-geometric approach for the Euler–Poincaré characteristic of spatial image. J Microsc 2000;198:54–62.
[31] Dequiedt AS, Coster M, Chermant L, Chermant JL. Study of phase dispersion in concrete by mage analysis. Cem Concr Comp 2001;23:215–26.
[32] Pinnamanemi BP, Lantuejoul C, Jernot JP, Chermant JL. Unbiased estimation of Euler–Poincaré characteristic. Acta Stereol 1989;8:101–6.
[33] Haas A, Matheron G, Serra J. Morphologie mathématique et granulométries en place. Ann Mines 1967;11:735–58.
[34] Haas A, Matheron G, Serra J. Morphologie mathématique et granulométries en place. Ann Mines 1967;12:767–82.
[35] Dequiedt AS, Coster M, Chermant L, Chermant JL. Distances between air-voids in concrete by automatic methods. Cem Concr Comp 2001;23:247–54.
[36] Pleau R, Pigeon M, Laurencot JL. Some findings on the usefulness of image analysis for determining the characteristics of the air-voids system on hardened concrete. Cem Concr Comp 2001;23:237–46.
[37] Stroeven P, Stroeven AP, Dalhuisen DH. Image analysis of "natural" concrete samples by automatic and manual procedures. Cem Concr Comp 2001;23:227–36.
[38] Boussa H, Tognazzi-Lawrence C, La Borderie C. A model for computation of leakage through damaged concrete structures. Cem Concr Comp 2001;23:279–87.
[39] Dequiedt AS, Coster M, Chermant JL, Jeulin D. Towards a model of concrete mesostructure. Cem Concr Comp 2001;23:289–97.
[40] Jeulin D, Monnaie P, Peronnet F. Gypsum morphological analysis and modeling. Cem Concr Comp 2001;23:299–311.
[41] Matheron G. Random sets and integral geometry. New York: Wiley; 1975.
[42] Jeulin D. Modèles morphologiques de structure aléatoires et de changement d'échelle. Thèse de Doctorat ès Sciences, University of Caen; 1991.
[43] Jeulin D. In: Jeulin D, editor. Advances in theory and application of random sets. Singapore: World Scientific; 1997.
[44] Chermant JL, Coster M. Material models and model materials. In: Wojnar L, editor. STERMAT, Sixth International Conference on Stereology and Image Analysis in Material Science, 20–23 Sept 2000; Krakow, Poland. Krakow: Fotobit Design; 2000: p. 17–36.
[45] Choquet G. Theory of capacities. Ann Inst Fourier 1953;5:131–295.
[46] Stoyan D, Kendall WS, Mecke J. Stochastic geometry and its applications. 2nd ed. NewYork: Wiley; 1995.
[47] Johnson WA, Mehl RF. Reaction kinetics in processes in nucleation and growth. Trans Am Inst Min Eng 1939;135:416–58.
[48] Miles RE. Poisson flats in euclidean spaces. Part 2: Homogeneous Poisson flats and the complementary theorem. Adv Probab 1971;3:1–43.
[49] Matheron G. Eléments pour une théorie des milieux poreux. Paris: Masson; 1967.
[50] Jeulin D. Dead leaves models: from spaces tessellation to random functions. In: Jeulin D, editor. Advances in theory and application of random sets. Singapore: World Scientific; 1997. p. 137–56.
[51] Stienen H. The sectionning of randomly dispersed particles, a computer simulation. Mikroscopie (Wien) 1980;S37:74–8.
[52] Saltykov SA. Stereometric metallography. Leipzig: VEB Deutscher Verlag für Grund-stoffindustrie; 1974 in German.
[53] Saltykov SA. Stereometric metallography. Moscow: Metallurgia; 1976 in Russian.
[54] Weibel ER. Stereological methods, vols. 1–2. London: Academic Press; 1980.
[55] Elias H, Hyde DM. A guide to practical stereology. Basel: Karger Pub Comp; 1983.
[56] Russ JC. Practical stereology. NewYork: Plenum Press; 1986.
[57] Exner HE, Hougardy HP. Quantitative image analysis of microstructure. Oberursel: DGM-Informationsgesellschaft Verlag; 1988.

[58] Säxl I. Stereology of objects with internal structure. Prague: Academia; 1989.
[59] Russ JC. Computer-assisted microscopy. The measurement and image analysis. NewYork: Plenum Press; 1990.
[60] Chassery JM, Montanvert A. Géometrie discrète en analyse d'images. Paris: Hermès; 1991.
[61] Schmitt M, Mattioli J. Morphologie mathématique. Paris: Masson; 1993.
[62] Coquerez JP, Philipp S. Analyse d'image: filtrage et segmentation. Paris: Masson; 1995.
[63] Säxl I, Pelikan K, Rataj J, Besterci M. Quantification and modelling of heterogeneous systems. Cambridge: International Science; 1995.
[64] Wojnar L. Image analysis. Applications in materials engineering. Boca-Raton, FL: CRC Press; 1998.